A Small Dielectric TEM Mode Resonator with a Crossing Slot And Its Application to a Cellular Radio VCO

Tomoki Uwano, *Member, IEEE*

***Abstract*—A small TEM mode dielectric resonator which has a new feature with a crossing slot on the outer ground conductor plane is presented. The slot, functioning as a short-ended stub line serially inserted into the transmission line, can tune the resonant frequency down. The resonant frequency in a stripline resonator structure is rigorously analyzed by the method based on the Spectral Domain Approach, and hence the equivalent circuit is derived. This resonator is applied to a cellular radio VCO with a varactor connected across the slot. The performance of the VCO in the 900 MHz cellular band is described.**

I. Introduction

SINCE a cellular telephone system was introduced as a mobile radio communication in the 800–900 MHz band a decade ago, circuit and device technology in this frequency band has rapidly advanced. Now design of small rf components and low power consumption semi-conductors allows realization of a handy telephone, which is expected to dominate the personal communication market in the near future. A dielectric TEM mode resonator is one of the key components which account for a low cost and down-sizing of a radio set. Most commonly used resonators are of a co-axial structure. It was first employed for antenna duplexers [1]. Relative permittivity ϵr of dielectrics used in their early stage was from 25 to 35 [2]. Then came dielectrics of ϵr 90, which shrunk the resonator even more. Further structural improvements were studied such as for stepped impedance structure to shorten the length [3] and frequency adjustment structure by combining a resonator with a trimming rotator [4]. Application of a co-axial resonator has also extended to a VCO. Taking advantage of relatively high Qu(unloaded Q), it is susceptible of a low phase noise performance. In a VCO, a varactor diode is connected to a resonator by a certain coupling means so that the frequency varies in the range from 2 to over 10%. Several planar resonators have been studied [5]–[7] for voltage tunable resonators.

Although its size is small, a stripline resonator has not been popular because of less performance advantage than the resonators mentioned. Down-sizing of a hand-held radio, however, has revived interest in stripline structure along with the technology of dielectric materials including multi-layer co-fired ceramics of high ϵr such as 75 [8].

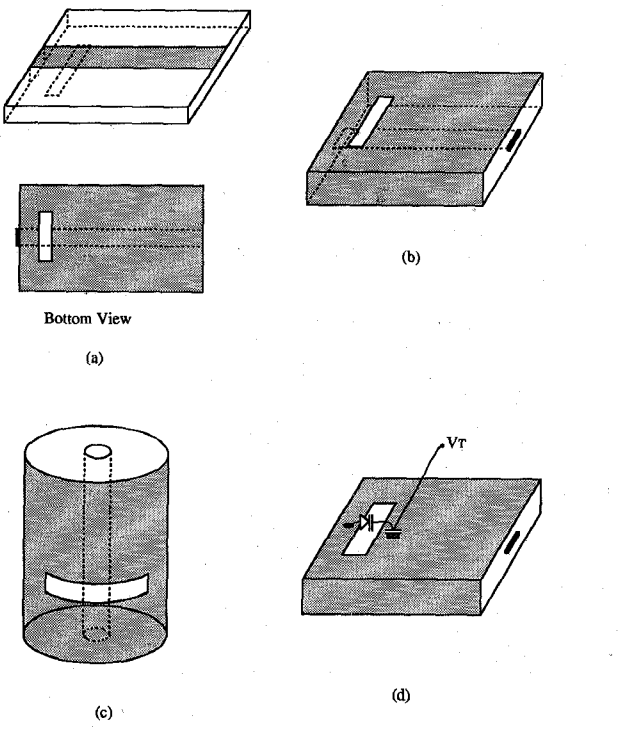

Fig. 1. Appearances of the presented TEM resonator with a crossing slot. (a) A microstrip line resonator. (b) A stripline with both sides shielded. (c) A coaxial resonator. (d) A frequency tunable structure with a varactor across the slot.

In this paper, a stripline resonator with a frequency tuning slot is studied. Fig. 1 (a)–(b) show the sketch of standard structures. In Fig. 1(a), a microstrip line forms a quarter wavelength resonator with one end grounded. The resonator should be 9 mm long when the dielectric ϵr is 90 in 900 MHz. On the ground conductor and in the proximity of the short-edge, there is a small slot crossing the stripline on the opposite side. The slot behaves as a short-ended transmission line serially inserted into the stripline at its crossing point. Thus, the resonance frequency can change in accordance with the slot length. The idea may extend to the structures as shown in Fig. 1(c)–(d). By connecting a varactor diode across the slot as illustrated, this resonator is voltage tunable and can be used for a VCO.

First part of this study describes the rigorous analysis of resonance frequency of the resonator by the method based

Manuscript received April 22, 1992; revised August 10, 1992.

T. Uwano is with Matsushita Electric Industrial Co., Ltd., Components and Devices Research Center, 1006 Oaza-kadoma, Kadoma, Osaka 571, Japan.

IEEE Log Number 9206306.

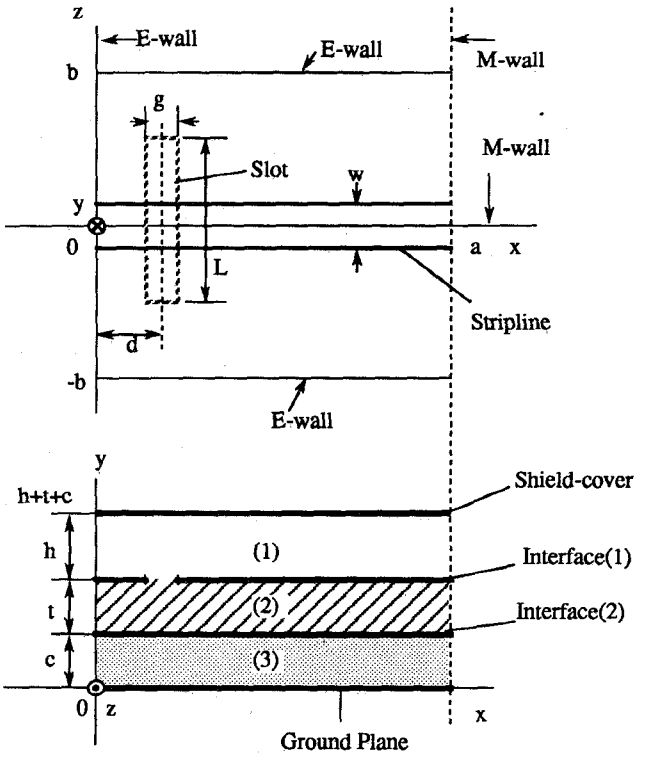

Fig. 2. A stripline structure of the problem.

on the Spectral Domain Analysis. An equivalent circuit is obtained to calculate the resonant frequencies of the resonator with a capacitor across the slot. Then, its application to a VCO is presented.

II. Resonator with a Slot

A. Analysis

Fig. 2 shows the structure to be analyzed for the resonators of Fig. 1(a) and (b) along with the coordinate system and dimensions. The structure is shielded at $y = 0, y = h + t + c$. A ground conductor and a slot are placed at the interface between layer 1 and 2 where the slot crosses perpendicularly the stripline. A stripline is placed at $y = c$. A resonator of Fig. 1(a) is one for which $h = c = \infty, \epsilon r1 = \epsilon r3 = 1$(air) and layer 2 is a dielectric substrate. Likewise, a resonator of Fig. 2(b) is one for which $h = \infty, \epsilon r1 = 1$ and layer 2 and 3 are dielectrics. Electric walls are assumed at $x = 0, z = \pm b$ and magnetic walls are assumed at $x = a, z = 0$.

In the Spectral Domain Analysis [9], the electric fields E and the currents J at each interface are expressed in a closed form as

$$\begin{bmatrix} \tilde{J}z^{(1)} \\ \tilde{J}x^{(1)} \\ \tilde{E}z^{(2)} \\ \tilde{E}x^{(2)} \end{bmatrix} = \begin{bmatrix} \tilde{Y}zz & \tilde{Y}zx & \tilde{T}zz & \tilde{T}zx \\ \tilde{Y}xz & \tilde{Y}xx & \tilde{T}xz & \tilde{T}xx \\ \tilde{S}zz & \tilde{S}zx & \tilde{Z}zz & \tilde{Z}zx \\ \tilde{S}xz & \tilde{S}xx & \tilde{Z}xz & \tilde{Z}xx \end{bmatrix} \begin{bmatrix} \tilde{E}z^{(1)} \\ \tilde{E}x^{(1)} \\ \tilde{J}z^{(2)} \\ \tilde{J}x^{(2)} \end{bmatrix} \quad (1)$$

where quantities with tildes $(\tilde{})$ are Fourier transforms of corresponding quantities. Number i in parenthesis refers to the interface (i) between layer i and $i + 1$. Including the image fields by the electric wall at $x = 0$, Fourier transform is defined between $[-a, a]$ and $[-b, b]$ as

$$\tilde{\Phi}(\alpha, \beta) = \int_{-b}^{b} \int_{-a}^{a} \Phi(x, y) e^{j(\alpha x + \beta z)}\, dx\, dz$$
$$\alpha = \frac{2m-1}{2a}\pi, \quad \beta = \frac{2n-1}{2b}\pi$$
$$m = 0, \pm 1, \pm 2 \cdots, n = 0, \pm 1, \pm 2 \cdots \quad (2)$$

In (1), $\tilde{E}^{(1)}$ are the electric fields over the slot and $\tilde{J}^{(2)}$ are the currents on the strip. Those are yet unknown quantities. $\tilde{J}^{(1)}$ and $\tilde{E}^{(2)}$ are to be eliminated by the Galerkin's process. Elements in the matrix are Green's functions to be obtained in the spectral domain formulation and are detailed in Appendix. $\tilde{J}^{(2)}$ and $\tilde{E}^{(1)}$ may be expanded in terms of known basis functions $J_{z\mu}, J_{x\mu}, E_{z\mu}$ and $E_{x\mu}$:

$$\tilde{J}_z(\alpha, \beta) = \sum_{\mu} a_\mu \tilde{J}_{z\mu}(\alpha, \beta),$$
$$\tilde{J}_x(\alpha, \beta) = \sum_{\mu} b_\mu \tilde{J}_{x\mu}(\alpha, \beta)$$
$$\tilde{E}_z(\alpha, \beta) = \sum_{\mu} c_\mu \tilde{E}_{z\mu}(\alpha, \beta),$$
$$\tilde{E}_x(\alpha, \beta) = \sum_{\mu} d_\mu \tilde{E}_{x\mu}(\alpha, \beta) \quad (3)$$

where a_μ, b_μ, c_μ and d_μ are unknown coefficients. The equation (1) is a function of resonant frequency ω_r. The problem can be solved by applying Galerkin's method. Thus, (1) is expressed as a homogeneous system of equations in terms of unknown coefficients vector:

$$\begin{bmatrix} K^{(11)} & K^{(12)} & K^{(13)} & K^{(14)} \\ K^{(21)} & K^{(22)} & K^{(23)} & K^{(24)} \\ K^{(31)} & K^{(32)} & K^{(33)} & K^{(34)} \\ K^{(41)} & K^{(42)} & K^{(43)} & K^{(44)} \end{bmatrix} \begin{bmatrix} c_\mu \\ d_\mu \\ a_\mu \\ b_\mu \end{bmatrix} = 0 \quad (4)$$

where

$$K_{ij}^{(11)} = \sum_{\alpha} \sum_{\beta} \tilde{E}z_i(\alpha, \beta)\, \tilde{Y}zz(\alpha, \beta)\, \tilde{E}z_j(\alpha, \beta)$$
$$\vdots$$
$$K_{ij}^{(44)} = \sum_{\alpha} \sum_{\beta} \tilde{J}x_i(\alpha, \beta)\, \tilde{Z}xx(\alpha, \beta)\, \tilde{J}x_j(\alpha, \beta)$$

In order that coefficient vector has non trivial solutions, the determinant of the matrix in (4) must be zero, and hence, ωr will be determined. For quick convergence, the basis functions may incorporate singular behavior of the fields normal to the edges of slot line and stripline. Thus, by assuming the electric and the magnetic wall, they are chosen as (5) shown at the bottom of the next page, where currents and fields are defined only on the strip and the slot and are zero elsewhere, and u, v, r, s are integer combinations chosen in accordance with μ. Transforms of those functions including image fields are obtained in Appendix.

Computed results of resonant frequencies for structures of Fig. 1(a) are shown in Fig. 3. Fig. 4 shows the experimental results of resonant frequencies for a microstrip structure with ceramic substrate of $\epsilon r = 90$, where the stripline and the ground conductor are made of fired silver thick film. The measured Qu values are also indicated in the graph.

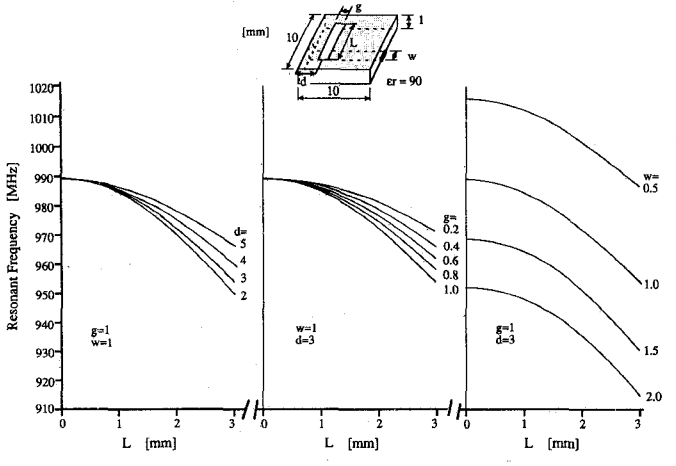

Fig. 3. Computed results of resonant frequencies in terms of the dimensions and the position of the slot for typical structures at the 900 MHz frequency band; a microstrip line on the substrate of $\epsilon r = 90$.

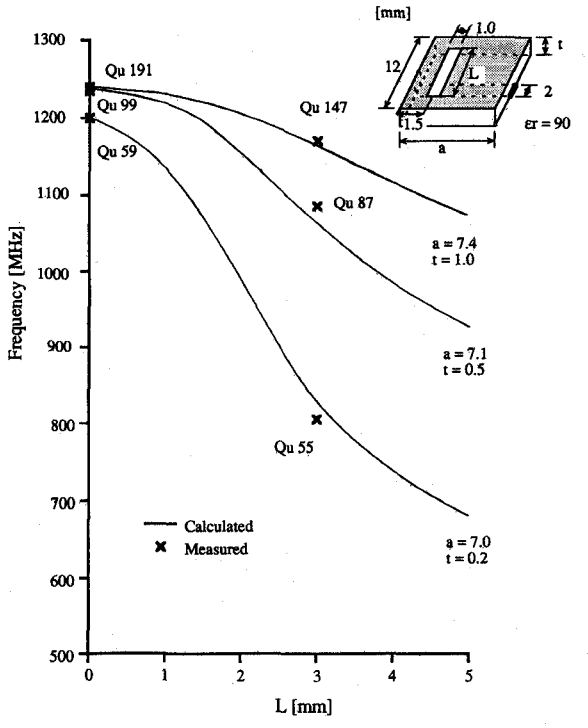

Fig. 4. Measured results of resonant frequencies and Qu's for the microstrip line resonator with the dimensional parameters shown in the figure.

B. Equivalent Circuit Representation

A crossing of stripline and slotline is a four-port circuit. The crossing can be solved and represented as an equivalent circuit either in a simple manner [10] or in a rigorous manner [11]. In this paper, since the discontinuity of a crossing is not an important subject to be solved, a simple equivalent circuit configuration from [10] will be used. Thus, the stripline resonator with a crossing slot is expressed as shown in Fig. 5(a). This equivalent circuit is also valid for the structures in Fig. 1(b)–(c) because the behavior of the fields in the proximity of a crossing is similar. In Fig. 5(a), a crossing is simply replaced by an ideal transformer with the impedance ratio of $n : 1$. The ratio n is frequency dependent. Then the equivalent circuit is replaced by Fig. 5(b).

The resonant frequency of the circuit in Fig. 5 is obtained from the equation

$$Zo - (Zo \tan \beta o\, d + nX) \tan \beta o(a - d) = 0$$

where

$$X = \frac{Zs}{2} \tan \beta s \frac{L}{2} \tag{6}$$

The Zs and βs of the slotline are calculated from an even mode structure of parallel coupled slotlines by assuming the

$$Jx_{uv}(x,z) = \cos\frac{2u-1}{2a}\pi x \frac{\cos\dfrac{2(v-1)}{w}\pi z}{\sqrt{1-\left(\dfrac{z}{w/2}\right)^2}} \qquad u,v = 1,2,3\cdots$$

$$Jz_{uv}(x,z) = \sin\frac{2u-1}{2a}\pi x \frac{\sin\dfrac{2v}{w}\pi z}{\sqrt{1-\left(\dfrac{z}{w/2}\right)^2}} \qquad u,v = 1,2,3\cdots$$

$$Ex_{rs}(x,z) = \cos\frac{2r-1}{L}\pi z \frac{1}{\sqrt{1-\left(\dfrac{x-d}{w/2}\right)^2}} \begin{cases} \cos\dfrac{s\pi}{g}(x-d) & s = 0,2\cdots \\ \sin\dfrac{s\pi}{g}(x-d) & s = 1,3\cdots \end{cases}$$

$$Ez_{rs}(x,z) = \sin\frac{2r-1}{L}\pi z \frac{1}{\sqrt{1-\left(\dfrac{x-d}{w/2}\right)^2}} \begin{cases} -\cos\dfrac{s\pi}{g}(x-d) & s = 1,3\cdots \\ \sin\dfrac{s\pi}{g}(x-d) & s = 2,4\cdots \\ & r = 1,2,3\cdots \end{cases} \tag{5}$$

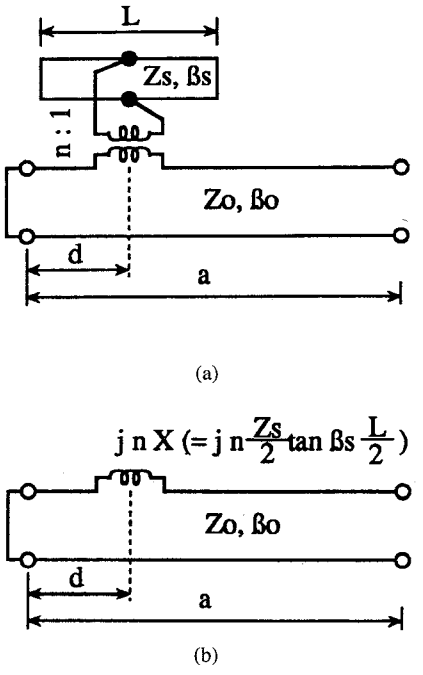

Fig. 5. An equivalent circuit of the resonator with a slot, where n refers to impedance ratio of a transformer, Zo and βo are characteristic impedance and propagation constant of a stripline, and Zs and βs are those of a slot. (a) A conventional expression with an ideal transformer. (b) A slot replaced by serially inserted inductance.

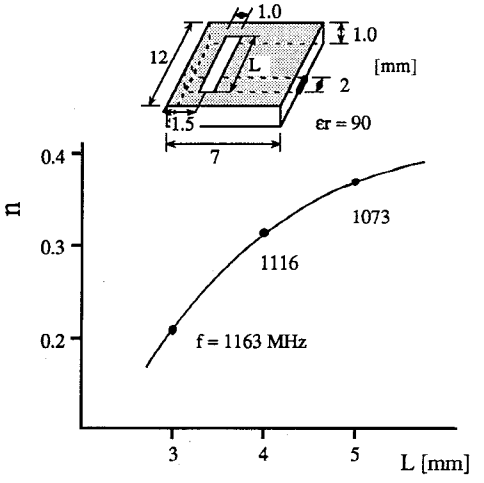

Fig. 6. Impedance ratios of the ideal transformer versus frequencies for the structure in the figure.

electric wall at $x = 0$. L should incorporate the edge effects of the parallel coupled slotline, which are also derived by the method based on SDA. Then, for the fixed resonant frequency, transcendental equation (6) is numerically solved for n. Fig. 6 shows the values of n versus frequencies for the structure illustrated in the figure.

From the equivalent circuit in Fig. 5, it is learned that the resonance frequency can change by the reactance (capacitance Cv) connected across the slot. This is illustrated in Fig. 7. The characteristic impedance, length and position of the slot provide a degree of freedom in terms of the frequency variation range for the same capacitance variation. Cv along with X makes the inserted inductive impedance higher to lower the

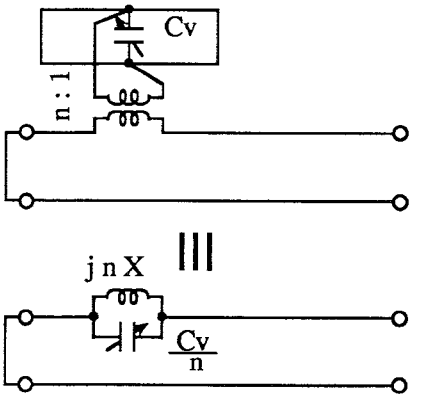

Fig. 7. An equivalent circuit of the resonator with a capacitor connected across the slot.

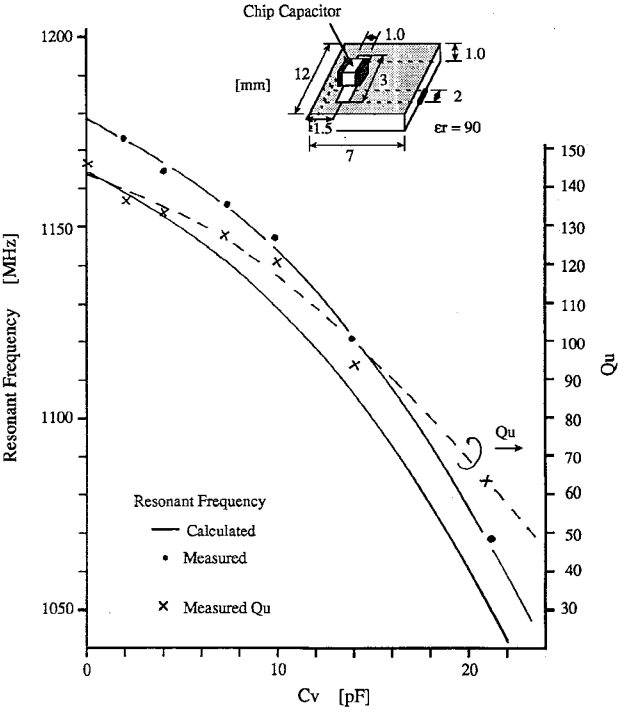

Fig. 8. Measured results of the resonant frequencies and Qu's versus capacitances across the slot.

resonant frequency. Thus, the resonant frequency in Fig. 7 is given by

$$Zo - (Zo \tan \beta o d + nX') \tan \beta o(a - d) = 0$$

where

$$X' = \frac{X}{1 - \omega X Cv} \tag{7}$$

Fig. 8 shows the measured results of the resonant frequencies versus Cv. Capacitors used in the experiment have the size of $1.0 \times 0.5 \times 0.5$ mm. Discrepancy between the measured and the calculated results from (7) using n in Fig. 6 is due to the dimensional inaccuracy of the length a. Except this, those results have an excellent agreement.

III. VCO Application

If the capacitor Cv is replaced by a varactor diode, the resonant frequency of the resonator is voltage-controlled. From Fig. 8, the frequency variation of 60 MHz is expected for the capacitance change from 10 to 20 pF with Qu value of more than 60. Expecting a good performance by those Qu, the presented resonator with a varactor diode was applied to a VCO. A varactor diode used in the experiment is encased in a so-called mini-mold package. Main characteristics of the diode is illustrated in Table I. The diode in the package has parasitic elements—mostly inductive ones—at connection conductor, and hence, its accurate equivalent circuit is difficult to be obtained. Although those elements would influence the frequency variation range in a sense at this frequency, it is supposed to be improved by adjusting the dimensions and the position of the slot. Fig. 9 illustrates the schematic of a VCO circuit. The oscillation circuit configuration and its element values are the same as those used in a commercially available VCO [Panasonic Electronic Components Catalog. ENF-VCO04]. First, the performance of the oscillation circuit was tested by connecting the standard dielectric co-axial resonator the Qu of which was known experimentally. The results of C/N (carrier to noise ratio) performance are shown in Fig. 10 with the theoretical curve derived from [12]. Incidentally, the C/N value corresponding to $Qu = 50$ is fairly approved one as an analog cellular VCO. Then the presented resonator was connected and the performance was measured. The diode is connected across the slot through a dc block capacitor of 9 pF. The measured results for the VCO are shown in Fig. 11–13. Fig. 11 illustrates the oscillation frequencies, output powers and C/N's regarding to the varactor voltage Vt. Despite that the frequency-voltage sensitivity over 10 MHz/2 V as in the graph is appropriate for a cellular radio use, the variation range is not as large as expected from the diode performance in Table I because of the parasitic inductances. The resonator in the experiment showed the first spurious resonance at the 20% higher frequency than the fundamental resonance, which is accounted for by those unnecessary elements. The spurious oscillation at this frequency, however, is avoided easily by selecting the feedback network capacitances in Fig. 9. The C/N performance with respect to the transistor collector currents is shown in Fig. 12. The results of C/N performance imply that the resonator maintained Qu's over 60. Instead of being connected usually to an open end of the resonator where the impedance is very high, the diode is connected to a low impedance circuit. Inevitably, the oscillation voltage bred at the diode terminals must be low. Hence, there are few chances that the oscillation voltage would give rise to rectified currents through the diode which might degrade the C/N performance. Fig. 13 illustrates the results of the C/N versus off-set carrier frequencies. In Fig. 13, 9 dB/oct curve (line) is observed which implies the $1/f$ noise characteristics below 3 KHz off-carrier, followed by 6 dB/oct curve. The crossing point frequency, 3 KHz, is where the flicker noise spectral density comes across that of shot noise in this transistor operation at the low frequency [12].

TABLE I
CHARACTERISTICS OF THE VARACTOR DIODE

		Typ.
Capacitance [pF]	1v	17 ~ 20
	2v	15
	10v	6
Rs [Ω]		0.18

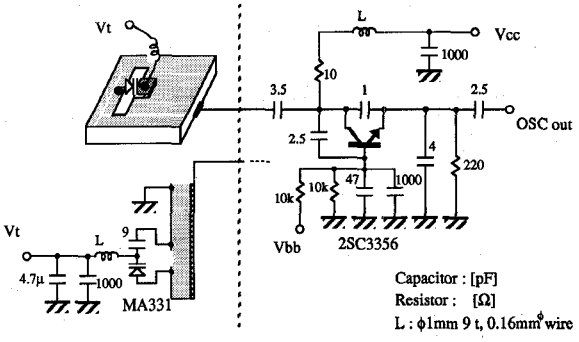

Fig. 9. A schematic of a VCO circuit.

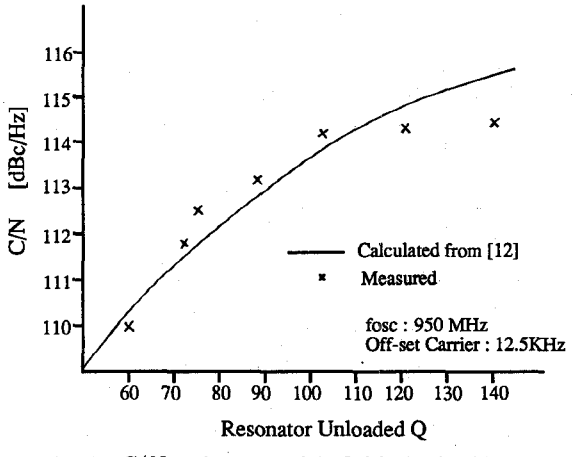

Fig. 10. Test for C/N performance of the VCO circuit with respect to Qu values of an attached resonator; $Vce = 3\,\mathrm{V}, Ic = 5$ mA.

In this experiment, the resonator of a microstrip line structure was used. To shrink the resonator, capacitive planar electrode at the open end or stepped impedance transmission line structure can be employed. In order to avoid electromagnetic radiation from the resonator, all-shielded structure as in Fig. 1(b) is favorable and practical. The low impedance at the varactor is susceptible of decreasing the radiation from the proximity of the diode. Thus, the presented idea of TEM mode resonator with a crossing slot extends to a miniature EMI free VCO.

IV. Conclusions

A stripline resonator with a crossing slot was rigorously analyzed by the method based on SDA. The resonant frequencies of the resonator were calculated with respect to the dimensions

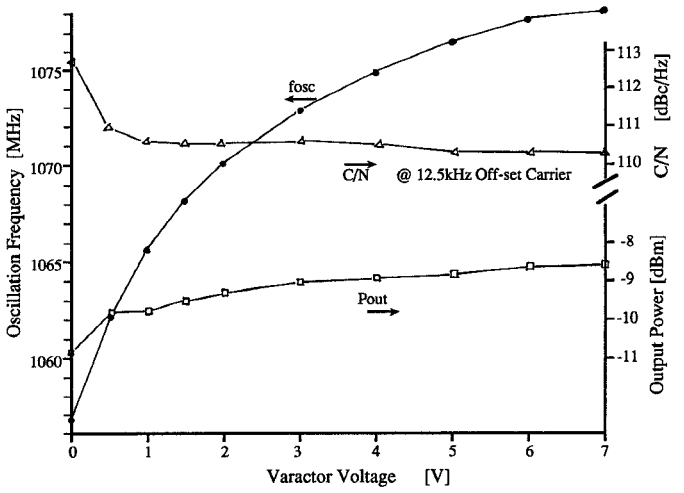

Fig. 11. Measured results of oscillation frequencies, output powers and C/N's versus varactor voltages for the VCO with the presented resonator being applied; $Vce = 3\,\mathrm{V}, Ic = 5$ mA.

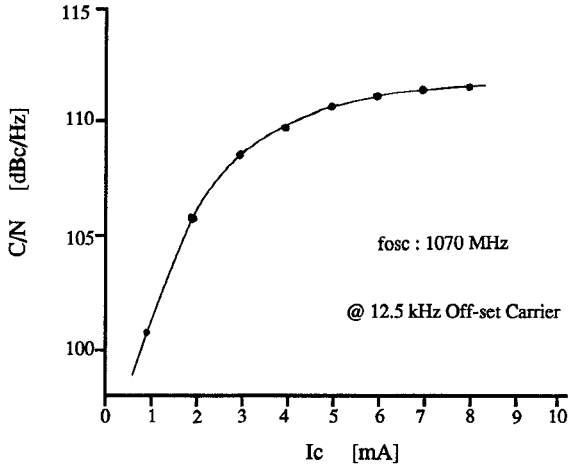

Fig. 12. Measured C/N performance with respect to transistor collector currents; $Vce = 3\,\mathrm{V}$, Varactor voltage $Vt = 2$ V.

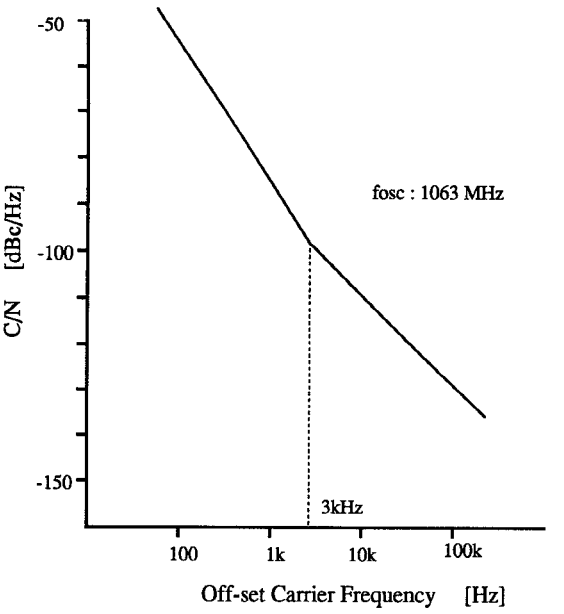

Fig. 13. Measured results of C/N's versus off-set carrier frequencies; $Vt = 0.6$ V.

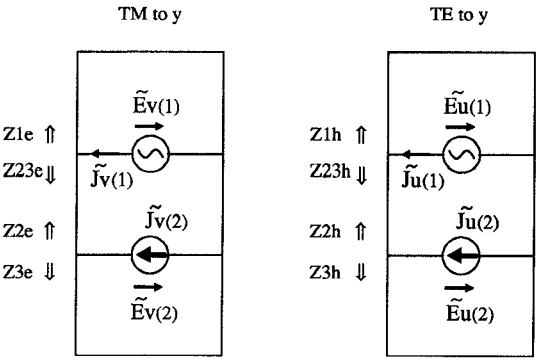

Fig. 14. Equivalent transmission lines for the TM and the TE fields.

and the position of the slot for a few structures. The equivalent circuit of the resonator was analytically derived, and hence the resonant frequencies of the resonator with capacitances connected across the slot were calculated and experimentally confirmed. Then the resonator with a varactor diode was applied to a VCO and its oscillation characteristics including C/N performance were measured. The results showed a very good performance for a cellular radio application.

APPENDIX

Derivation of Field Equations

The structure in Fig. 2 is inhomogeneous in y. The field equations are derived by the Immittance Approach in the SDA [9], where fields are a superposition of the inhomogeneous (in y) plane waves created by $\tilde{E}v^{(1)}$, $\tilde{J}v^{(2)}$, $\tilde{E}u^{(1)}$ and $\tilde{J}u^{(2)}$ in the (u, v) coordinate system. Coordinate relations between (u, v) and (x, y) are

$$u = z\sin\theta - x\cos\theta \qquad v = z\cos\theta + x\sin\theta$$
$$\cos\theta = \frac{\beta}{\sqrt{\alpha^2+\beta^2}} \qquad \sin\theta = \frac{\alpha}{\sqrt{\alpha^2+\beta^2}} \tag{A1}$$

$\tilde{J}v$ and $\tilde{E}v$ create only the TM (to y) fields and $\tilde{J}u$ and $\tilde{E}u$ create the TE (to y) fields. Hence, equivalent circuits for the TM and TE fields are obtained from the transmission line analogy as shown in Fig. 14. First, the wave impedances looking from the location of the sources are found. Then the fields equations for $\tilde{J}v^{(1)}$ and $\tilde{E}v^{(2)}$ are obtained as a superposition of the fields by two sources $\tilde{E}v^{(1)}$ and $\tilde{J}v^{(2)}$, and likewise $\tilde{J}u^{(1)}$ and $\tilde{E}u^{(2)}$ are given by $\tilde{E}u^{(1)}$ and $\tilde{J}u^{(2)}$. The directions of the current and the voltage vectors in Fig. 14 are defined from the characteristics of the wave impedances. Substitution of those u, v field components into (A1) yields x, y field components for (1). Thus, the matrix elements in

$$
\begin{aligned}
v &= -(\alpha^2+\beta^2)^{-1}\\
\tilde{Y}1^e &= \frac{\gamma y_1\gamma y_2 Ct_2 Ct_3+\gamma y_2^2 Ct_1 Ct_3+\gamma y_2\gamma y_3 Ct_1 Ct_2+\gamma y_1\gamma y_3}{\gamma y_1\gamma y_2(\gamma y_2 Ct_3+\gamma y_3 Ct_2)}\\
\tilde{Y}1^h &= \frac{\gamma z_1\gamma z_2 Ct_1 Ct_2+\gamma z_1\gamma z_3 Ct_1 Ct_3+\gamma z_2\gamma z_3 Ct_2 Ct_3+\gamma z_2^2}{\gamma z_2 Ct_2+\gamma z_3 Ct_3}\\
\tilde{Z}t^e &= \frac{\gamma y_3}{S_2(\gamma y_2 Ct_3+\gamma y_3 Ct_2)}, \qquad \tilde{Z}t^h = \frac{\gamma z_2}{S_2(\gamma z_2 Ct_2+\gamma z_3 Ct_3)}\\
\tilde{Z}s^e &= \frac{\gamma y_2\gamma y_3}{\gamma y_2 Ct_3+\gamma y_3 Ct_2}, \qquad \tilde{Z}s^h = \frac{1}{\gamma z_2 Ct_2+\gamma z_3 Ct_3}\\
\gamma y_i &= \gamma_i/\hat{y}_i, \quad \gamma z_i = \gamma_i/\hat{z}_i, \quad \hat{y}_i = j\omega\epsilon_i, \quad \hat{z}_i = j\omega\mu_i\\
k_i^2 &= -\hat{y}_i\hat{z}_i, \quad \gamma_i^2 = \alpha^2+\beta^2-k_i^2, \quad \text{Subscript } i \text{ refers to layer } i. \qquad i=1,2,3\\
Ct_1 &= \coth\gamma_1 h, \quad Ct_2 = \coth\gamma_2 t, \quad Ct_3 = \coth\gamma_3 c, \quad S_2 = \sinh\gamma_2 t,
\end{aligned}
$$

$$
\begin{aligned}
Px &= \frac{w}{2}\beta+(v-1)\pi, \quad & Pw &= \frac{w}{2}\beta+v\pi, \quad & Ps &= \frac{g}{2}\beta+\frac{s-1}{2}\pi, \quad & Pg &= \frac{g}{2}\beta+\frac{s}{2}\pi\\
Qx &= \frac{w}{2}\beta-(v-1)\pi, \quad & Qw &= \frac{w}{2}\beta-v\pi, \quad & Qs &= \frac{g}{2}\beta-\frac{s-1}{2}\pi, \quad & Qg &= \frac{g}{2}\beta-\frac{s}{2}\pi\\
A &= \frac{2r-1}{2lh}-\beta, & B &= \frac{2r-1}{2lh}+\beta, & L &= 2lh
\end{aligned}
$$

(1) are

$$
\begin{aligned}
&\tilde{Y}zz = v(\beta^2\tilde{Y}1^e+\alpha^2\tilde{Y}1^h) && \tilde{Y}zx = v\alpha\beta(\tilde{Y}1^e-\tilde{Y}1^h)\\
&\tilde{Y}xz = \tilde{Y}zx && \tilde{Y}xx = v(\alpha^2\tilde{Y}1^e+\beta^2\tilde{Y}1^h)\\
&\tilde{T}zz = v(\beta^2\tilde{Z}t^e+\alpha^2\tilde{Z}t^h) && \tilde{T}zx = v\alpha\beta(\tilde{Z}t^e-\tilde{Z}t^h)\\
&\tilde{T}xz = \tilde{T}zx && \tilde{T}xx = v(\alpha^2\tilde{Z}t^e+\beta^2\tilde{Z}t^h)\\
&\tilde{S}zz = -\tilde{T}zz && \tilde{S}zx = -\tilde{T}zx\\
&\tilde{S}xz = -\tilde{T}xz && \tilde{S}xx = -\tilde{T}xx\\
&\tilde{Z}zz = v(\beta^2\tilde{Z}s^e+\alpha^2\tilde{Z}s^h) && \tilde{Z}zx = v\alpha\beta(\tilde{Z}s^e-\tilde{Z}s^h)\\
&\tilde{Z}xz = \tilde{Z}zx && \tilde{Z}xx = v(\alpha^2\tilde{Z}s^e+\beta^2\tilde{Z}s^h)
\end{aligned}
$$

where the first equation at the top of the page is true.

Fourier Transforms of (5)

$$
\tilde{J}x_{uv}(\alpha,\beta) = \begin{cases} \frac{w}{4}\pi[Jo(Px)+Jo(Qx)]a & \alpha = \pm\frac{2m-1}{2a}\pi\\ 0 & \alpha \neq \pm\frac{2m-1}{2a}\pi \end{cases}
$$

$$
\tilde{J}z_{uv}(\alpha,\beta) = \begin{cases} \frac{w}{4}\pi[Jo(Pw)-Jo(Qw)]a & \alpha = \frac{2m-1}{2a}\pi\\ -\frac{w}{4}\pi[Jo(Pw)-Jo(Qw)]a & \alpha = -\frac{2m-1}{2a}\pi\\ 0 & \alpha \neq \pm\frac{2m-1}{2a}\pi \end{cases}
$$

$$
u, v = 1, 2\cdots
$$

$$
\begin{aligned}
\tilde{E}x_{rs}(\alpha,\beta) =& \frac{g}{2}\pi\left[\frac{1}{A}\sin Alh+\frac{1}{B}\sin Blh\right]\\
&\cdot[Jo(Ps)+(-1)^{s-1}Jo(Qs)]\\
&\cdot\begin{bmatrix}\cos\alpha d & s=1,3\cdots\\ \sin\alpha d & s=2,4\cdots\end{bmatrix}\\
\tilde{E}z_{rs}(\alpha,\beta) =& \frac{g}{2}\pi\left[\frac{1}{A}\sin Alh-\frac{1}{B}\sin Blh\right]\\
&\cdot[Jo(Pg)+(-1)^{s-1}Jo(Qg)]\\
&\cdot\begin{bmatrix}\sin\alpha d & s=1,3\cdots\\ \cos\alpha d & s=2,4\cdots\end{bmatrix}\\
& r = 1,2\cdots
\end{aligned}
$$

where the second equation at the top of the page is true with Jo the zero-order Bessel function of the first kind.

ACKNOWLEDGMENT

The author wishes to thank Dr. T. Nagasawa, the director of the Components and Devices Research Center, for giving the opportunity of this work, and T. Ishida, the director of the Materials and Components Research Laboratory, for continuous encouragement. The author would also like to thank Y. Nakagawa for his expert help with the fabrication and the experiments of the VCO.

REFERENCES

[1] K. Wakino *et al.*, "Quarter wave dielectric transmission line duplexer for land mobile communications," in *IEEE MTT-S Int. Microwave Symp. Dig.*, June 1979, pp. 278–280.

[2] S. Kawashima *et al.*, "Ba($Zn_{1/3}Ta_{2/3}$)O_3 ceramics with low dielectric

loss at microwave frequencies," *J. American Ceramic Society,* vol. 66, no. 6, June 1983.
[3] M. Sagawa, M. Makimoto, and S. Yamashita, "A design method of bandpass filters using dielectric-filled coaxial resonators," *IEEE Trans. Microwave Theory Tech.,* vol. MTT-33, no. 2, pp. 152–157, Feb. 1985.
[4] T. Uwano, "Ceramic-filled resonator cuts costs of radio-telephone filters," *Electronics,* McGraw-Hill, July 14, 1983.
[5] K. Kawamoto, K. Hirota, N. Niizaki, Y. Fujiwara, and K. Ueki, "Small Size VCO module for 900 MHz using coupled microstrip-coplanar lines," in *IEEE MTT-S Int. Microwave Symp. Dig.,* June 1985, pp. 689–692.
[6] K. Chang, S. Martin, F. Wang, and J. L. Klein, "On the study of microstrip ring and varactor-tuned ring circuits," *IEEE Trans. Microwave Theory Tech.,* vol. MTT-35, no. 12, pp. 1288–1295, Dec. 1985.
[7] M. Makimoto and M. Sagawa, "Varactor tuned bandpass filters using microstrip-line ring resonators," in *IEEE MTT-S Int. Microwave Symp. Dig.,* June 1986, pp. 411–414.
[8] T. Okawa and H. Utaki, "Development of multilayer dielectric filter using low temperature fired microwave ceramics," *Sumitomo Metals,* vol. 43, no. 4, 1991, pp. 134–138 (in Japanese).
[9] T. Itoh, *Numerical Techniques for Microwave and Millimeter-Wave Passive Structures.* New York: Wiley-Interscience, 1989, ch. 5.
[10] K. C. Gupta, R. Garg, I. J. Bahl, *Microstrip Lines and Slotlines.* Norwood, MA: Artech House, 1979.
[11] T. Uwano, T. Itoh, and R. Sorrentino, "Characterization of microstrip-to-slotline transition discontinuities by transverse resonance analysis," *Alta Frequenza,* vol. LVII-N.5 June 1988, pp. 183–191.
[12] D. B. Leeson, "A simple model of feedback oscillator noise spectrum," *Proc. IEEE,* vol. 54, pp. 329–330, Feb. 1966.

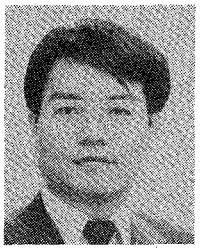

Tomoki Uwano (M'87) was born in Toyama, Japan, on October 18, 1948. He received the B.S. degree from the Tokyo Institute of Technology in 1971.

Since 1971, he has been employed by the Matsushita Electric Ind. Co., Ltd, Osaka, Japan, where he has been engaged in research and development on microwave and millimeter-wave circuitry, satellite and cellular radio communications. From April 1985 to December 1986, he was a Visiting Scholar in the Department of Electrical and Computer Engineering of the University of Texas at Austin.

Mr. Uwano is a member of the Institute of Electronics, Information and Communication Engineers of Japan.